Chemical Geology 320–321 (2012) 128–139

Contents lists available at SciVerse ScienceDirect

Chemical Geology

journal homepage: www.elsevier.com/locate/chemgeo

Research paper

He-Ar-H-O isotopic signatures in Au – Ag bearing ore fluids of the Sunshin epithermal gold-silver ore deposits, South Korea

Kyu Han Kim [a,*], Seungyeol Lee [b], Keisuke Nagao [c], Hirochika Sumino [c], Kyounghee Yang [b], Jong Ik Lee [d]

[a] Department of Science Education, Ewha Womans University, Seoul 120-750, South Korea
[b] Pusan National University, Geumjeong-gu, Busan 609-735, South Korea
[c] Geochemical Research Center, Graduate School of Science, University of Tokyo, Tokyo 113-0033, Japan
[d] Korea Polar Research Institute, KORDI, Songdo Techno Park, Incheon 406-840, South Korea

ARTICLE INFO

Article history:
Received 22 October 2011
Received in revised form 25 May 2012
Accepted 29 May 2012
Available online 4 June 2012

Editor: L. Reisberg

Keywords:
Mantle helium
Fluid inclusions
Oxygen isotopes
Epithermal gold-silver ore deposits
Sunshin gold-silver deposits

ABSTRACT

Helium ($^3He/^4He$), argon ($^{40}Ar/^{36}Ar$) and oxygen ($^{18}O/^{16}O$) isotopic ratios in fluid inclusions trapped in quartz and pyrite from the Sunshin epithermal gold-silver ore deposits in South Korea were analyzed to investigate the magmatic contribution to ore forming fluids. Mantle helium with high $^3He/^4He$ ratios (up to $^3He/^4He \sim 9R_A$, where $R_A = 1.4 \times 10^{-6}$ for air) were identified from fluid inclusions in auriferous quartz veins, which are characterized as low sulfidation (adularia-sericite) type. The ratios provide direct evidence of links between low sulfidation ore fluids in epithermal gold deposits and magma from a mantle source. Interestingly, the oxygen and hydrogen isotopic compositions of the ore fluids ($\delta^{18}O = -1.9$ to $-6.6‰$, $\delta D = -82$ to $-100‰$), calculated from ore quartz, indicate that meteoric waters were predominant during precipitation of the Au – Ag ore. Microthermometric measurements for fluid inclusions indicate relatively low temperatures (≤ 300 °C) for the formation of the low sulfidation epithermal ore deposits.

1. Introduction

Mineralizing fluids involved in the formation of epithermal gold-silver ore deposits may be classified by their distinct sources: magmatic fluids, deeply circulating meteoric water (crustal water), sedimentary brines and shallow meteoric waters (Albinson et al., 2000). In general, epithermal gold-silver deposits may be genetically divided into three types: low sulfidation (adularia-sericite), intermediate sulfidation and high sulfidation (acid sulfate, pyrite-alunite-H_2S-SO_4) (White and Hedenquist, 1990; Cooke and Simmons, 2000). Volcanic-hosted hydrothermal systems are ultimately driven by magmatic intrusions, even though they do not exhibit obvious links to magma (Morishita and Nakano, 2008). High sulfidation Au deposits most likely are derived from fluids released directly from a freely boiling underground magma chamber. Therefore, a direct magmatic contribution to gold-silver ore formation processes has been proven in the case of high sulfidation ore deposits (e.g., Hedenquist and Lowenstern, 1994; Hedenquist et al., 2000; Deyell et al., 2005; Rainbow et al., 2005). In contrast, low sulfidation epithermal ore deposits (LSEOD) are formed near the surface in groundwater-dominated hydrothermal systems where magmatic fluid has not been directly involved (Giggenbach, 1997; Hedenquist et al., 2000). Therefore, the magmatic signature associated with LSEOD, which encompass 65% of the principal gold ore deposits in the Western Pacific island arcs (Sillitoe, 1987), is elusive and remains unclear (Heald et al., 1987; Cooke and Simmons, 2000; John, 2001; Camprubi et al., 2006; Morishita and Nakano, 2008; Zhang et al., 2010).

The aim of the present study is to discover if there is evidence of a magmatic source for ore forming fluids in low sulfidation Au – Ag mineralization by analyzing noble gas isotopes (He – Ar) trapped in fluid inclusions of ore quartz and pyrite. Noble gases preserved in fluid inclusions are sensitive indicators of the source of hydrothermal fluids (Stuart and Turner, 1992; Stuart et al., 1995; Burnard and Polya, 2004). To search for evidence of a magmatic signature we studied the Sunshin LSEOD. The Sunshin gold-silver ore deposits are currently being intensively mined for Au and Ag in the Haenam metallogenic province. These deposits have no previously documented geochemical affinity with a magmatic source. Isotopic analyses of the Tongyoung and Kwangyang epithermal type gold deposits, which occur in a similar tectonic setting to the Sunshin deposits, are included for comparison purposes (Fig. 1).

2. Geologic setting and ore deposits

The Sunshin gold-silver deposits are located in the Haenam-Jindo volcanic-sedimentary basin, South Korea (Fig. 1). This Cretaceous non-marine basin consists of four volcanic-sedimentary sequences:

* Corresponding author. Tel.: +82 2 3277 2696; fax: +82 2 3277 2685.
E-mail address: kyuhan@ewha.ac.kr (K.H. Kim).

0009-2541/$ – see front matter © 2012 Elsevier B.V. All rights reserved.
doi:10.1016/j.chemgeo.2012.05.027

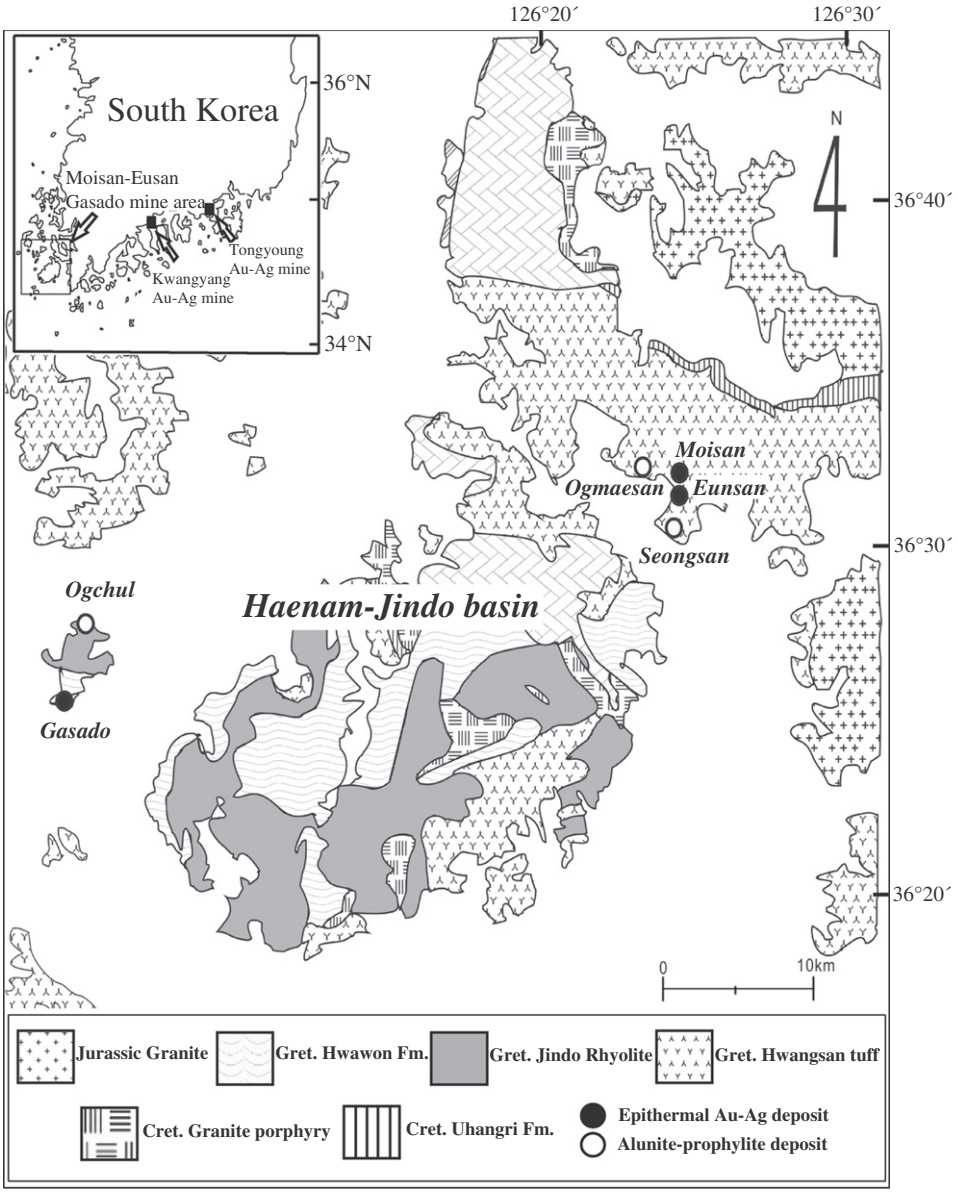

Fig. 1. Geologic map of the Sunshin epithermal Au – Ag ore deposits with sample sites identified. The Eunsan, Moisan, and Gasado deposits occur in the Haenam-Jindo volcano-sedimentary basin (Geologic map after Choi et al., 2005). Sampling locations: Eunsan: 126° 24′ 20″E, 36° 31′ 40″N, Moisan: 126° 24′ 05″E, 36° 32′ 05″N, Gasado: 126° 02′ 30″E, 27° 45′ 20″N, Tongyoung: 128° 26′ 04″E, 34° 50′ 08″N, Kwangyang: 127° 37′ 00″E, 35° 55′ 50″N.

the lower andesitic tuff of the Hwawon Formation (95.4–92.7 Ma), a volcanoclastic and epiclastic shallow lacustrine sedimentary sequence (Uhangri Formation, 400 m thick), dacitic tuff (Hwangsan Tuff, 86.4–81.4 Ma), and rhyolite (Jindo Rhyolite, 76.3–66.2 Ma) in ascending order (Chough et al., 1996; Chun and Chough, 1995, Fig. 1). These volcano-sedimentary formations overlie Jurassic basement and were intruded by Cretaceous granitic rocks and felsic igneous rocks. The Sunshin gold-silver deposits are hosted in the Cretaceous felsic pyroclastics and sedimentary rocks of the Hwangsan Formation, which formed in response to subduction of the Izanagi oceanic plate (Choi et al., 2005). The Hwangsan Formation consists mainly of dacitic to rhyolitic tuffs and carbonaceous shale. The Tongyoung and Kwangyang gold deposits are located in a volcano-sedimentary basin in the vicinity of the Haenam-Jindo basin and are also known as epithermal type gold deposits (Kim and Shin, 1989; Shelton et al., 1990; Park et al., 2001).

2.1. Gold ore deposits

The Sunshin LSEODs are comprised of three sets of Au – Ag bearing epithermal ore deposits, the (1) Eunsan, (2) Moisan and (3) Gasado deposits. The Eunsan and Moisan deposits are located in close proximity while the Gasado deposit is 35 km away from the Eunsan deposit. They have quite similar geological characteristics in terms of occurrence, ore and host rock geology, and age of mineralization (Table 1, Fig. 1).

Currently only the Eunsan and Moisan ore deposits are actively being worked to produce Au and Ag. The Gasado mine is closed. The main orebodies of the deposits consist of sheeted and stockwork quartz veins embedded along fissure and fault fractures in rhyolitic and tuffaceous volcanic rocks. The volcanic rocks were generated at relatively shallow levels, as found from the H_2O content of a glass inclusion (ca. 2–4 wt.%) found in a quartz phenocryst from the tuff. The H_2O content

Table 1
Summary of geological and mineralogical features of the Ensan, Moisan and Gasado deposits.

Ore deposits	Eunsan	Moisan	Gasado
Host rocks	Rhyolitic, dacitic, tuffaceous rocks, carbonaceous shale	Rhyolitic, dacitic, andesitic and tuffaceous rocks	Dacitic tuff
Associated metal	Au, Ag, Pb, Zn, Mn	Au, Ag, Cu, Bi	Au, Ag, Cu, Pb, Zn
Ore vein system	Fissure > sheeted	Sheeted ≥ fissure	Fissure, sheeted and stockwork
Ore vein mineralogy	Pyrite, chalcopyrite, galena sphalerite, tennantite, argentite, Ag-rich electrum	Chalcopyrite, pyrite, sphalerite, galena bismuthinite, Au-rich electrum,	Chalcopyrite, sphalerite, galena, pyrite argentite, electrum, Quartz, adularia, calcite
	Quartz, adularia, calcite, clay minerals	Quartz, adularia, calcite	
Alteration	Sericitic	Sericitic, chloritization, propylitic	Advanced argillic, argillic phyllic, propyilitic
Homogenization temperature	136–310 °C	146–289 °C	158–285 °C (Kim et al., 2002)
Age of mineralization	75.0 ± 1.6 Ma (Kim, 2011)	75.1 ± 1.6 Ma (Kim, 2011)	70.5 Ma (Koh et al., 2000)

suggests a water saturation pressure (P_{H2O}) of about 300–900 bars, corresponding to a minimum depth of 0.8–2.5 km for the magma chamber (Lee et al., 2009). Choi et al. (2005) reported that the homogenization temperatures of fluid inclusions in quartz from the Eunsan and Moisan deposits range from 113–298 °C and 133–319 °C respectively with relatively low salinities of <1.7 wt.% NaCl equivalent. Meanwhile, the homogenization temperatures of fluid inclusions in the Gasado vein quartz range from 158 to 285 °C, with corresponding salinities of 0.9 to 3.4 wt.% NaCl equivalent (Kim et al., 2002). It is interesting to note that the Eunsan deposits (Se-type) formed at the upper level of the epithermal system at relatively low temperature compared to the Moisan deposits (Te-type) (Choi et al., 2005). Selenium partially substitutes for sulfur in many sulfides due to its similar geochemical properties and it may form independent selenium minerals in low temperature low sulfur fugacity environments. In contrast, tellurium does not replace sulfur due to the large difference in ionic radius between tellurium and sulphur (Smirnov et al., 1983). As anionic selenium is immobilized by reduction, deposits tend to be concentrated in organic matter-rich sediments. Therefore, selenium is mainly found in the black shale, which hosts the Se-type epithermal gold deposits. These shales never host the Te-type deposits, which are formed closer to the center of volcanic activity (Shikazono, 2003).

Radiometric ages (whole rock K–Ar) of arc volcanism in the Haenam-Jindo basin range from 100 to 65 Ma, with a major population between 85 and 70 Ma (Moon et al., 1991; Kim and Nagao, 1992). K–Ar ages of mineralization for the Eunsan and Moisan deposits are 75.0 ± 1.6 Ma (adularia) and 75.1 ± 1.6 Ma (sericite), respectively (Kim, 2011). The K–Ar dating of sericites from the Gasado gold deposits suggests a restricted age range of 70.5–70.1 Ma, regarded as the main age of epithermal Au–Ag mineralization in this area (Koh et al., 2000). Both adularia and sericite ages overlap the age of main arc volcanism in the Cretaceous Haenam-Jindo basin.

To compare the isotopic characteristics of the Sunshin deposits with those of other epithermal ore deposits that occur in a similar tectonic setting, samples from the Tongyoung and Kwangyang gold deposits, were included for He isotopic analysis. The Tongyoung Au–Ag veins were emplaced in andesite of Cretaceous age, while the Kwangyang gold bearing quartz veins are embedded in Precambrian gneiss.

2.2. Characteristics of vein systems

2.2.1. The Eunsan deposit

The Eunsan Au–Ag bearing quartz veins are traced intermittently for more than 350 m along strike, extend 100–150 m, vary considerably in thickness from 0.01 to 1.3 m and dip 60–80° in a NW direction (Aung, 2004). The veins can be considered as a single ore mineralized zone (Fig. 2). The occurrence of ore enriched vein structures is more pronounced and concentrated towards the contact between the hydrothermally brecciated rocks and overlying tuffs. The northwest trend of the ore veins reaches to the Ogmaesan clay and alunite deposits, currently the most active pyrophyllite-alunite producing ores in South Korea. Generally, gold and silver minerals, accompanied by sulfides, are more concentrated in dark grey layers of the quartz veins as shown in Fig. 3A. The 2002 annual production figures for the Eunsan deposit were 168 kg Au and 6755 kg Ag (Choi et al., 2005).

Most epithermal veins comprise bladed quartz and crudely colloform to cockade-banded quartz, chalcedony, adularia and carbonate minerals, with lesser illite-smectite, adularia, and sulfide bands in which base metal sulfides are only minor components (Fig. 3C).

2.2.2. The Moisan deposit

The Moisan deposit consists of several epithermal quartz veins (Fig. 2). The four major lens-shaped veins forming the presently

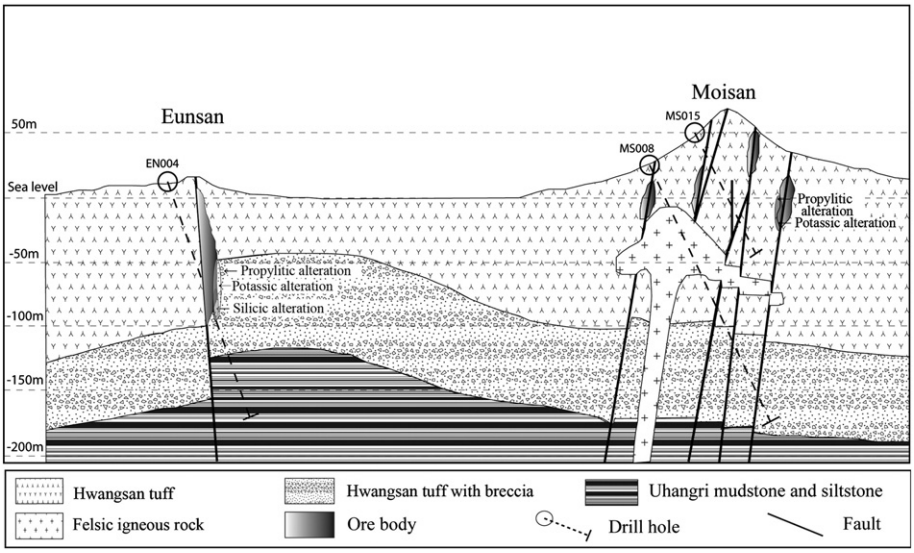

Fig. 2. Generalized cross-section of Au veins at the Eunsan (A) and Moisan (B) gold deposit.

economic part of the deposit are located about 1 km north of the Eunsan deposits. The deposits have developed in epithermal quartz veins that display low temperature epithermal fissure-filling textures including crustiform banding and hydrothermal breccias as shown in Fig. 3B and D. Brecciated and bladed textures with comb and cockade texture suggest that, the Moisan deposit, unlike the Eunsan, does not show decisive evidence of boiling in the near surface environment. Instead it seems likely that the Moisan deposit only experienced very weak boiling (Kim, 2011). The Au – Ag bearing veins vary from 0.01 to 0.5 m in width and extend to more than 550 m depth. The trend of the Moisan ore veins is N55W with a dip of 60-80SW. The drill core samples of Moisan veins have ore grades of ND-493 g/t for gold and ND-1300 g/t for Ag (Aung, 2004).

2.2.3. The Gasado deposit

The Gasado gold-silver deposit is also principally composed of fissure-filling veins of low sulfidation type. The Au – Ag veins occur in the propylitically altered late Cretaceous dacitic tuff formation of the southern part of Gasado island, striking from N10 to 60E, dipping from 65-70NE and with a maximum width of 7–8 m. The ore veins form a sheeted and stockwork system. The eight major ore veins associated with chalcedonic, comb, brecciated and vuggy structures, are controlled by NE or NS trending small scale faults. The size of the gold bearing-veins varies considerably from 0.5 cm to 1 m in thickness and 50 to 500 m in length. They extend to a depth of less than 200 m below sea level, with grades of 2.3 g/t Au and 109.9 g/t Ag recorded from the Lighthouse ore vein (Kim et al., 2002).

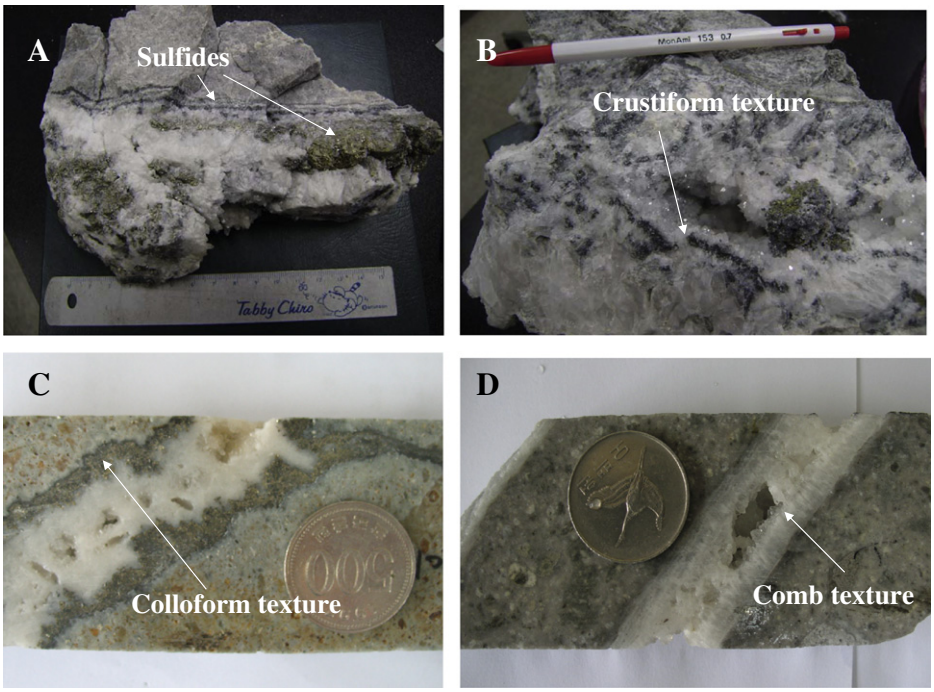

Fig. 3. Vein textures associated with Au – Ag mineralization from the Eunsan and Moisan gold deposits. Banded structures consist of chalcedony and electrum bearing pyrites and quartz from the Eunsan deposits (A). Vuggy quartz and crustiform structures with electrum bearing pyrites are from Moisan deposits (B). (C) Milky chalcedonic to crystalline quartz veins crosscutting the host rocks. (D) Crystalline quartz with comb structure showing crustiform habit.

2.3. Vein mineralogy

The vein stratigraphy of the Sunshin deposits can be grouped into three mineralization stages. Stage I is dominated by a quartz-pyrite sulfide association, whereas Stage II contains most of the precious metal sulfide assemblages, the economically important paragenetic sequence, and Stage III is dominated by carbonate (Fig. 4). Stages I and II were terminated by the onset of a fracturing and brecciation event and are overprinted by barren calcite veining (Aung, 2004). The mineralogy of the ore-bearing veins is characterized by a dominance of Ag-As-Sb sulfosalts, accompanied by Ag-selenides and tellurides, over argentite (Choi et al., 2005). Base metal sulfides, together with gold minerals, precipitated early in all mineralization stages. On the other hand, Ag-bearing sulfides, sulfosalts or selenides precipitated at a later stage of mineralization.

Ore mineralogy in the Moisan and Eunsan deposits is relatively simple, and is represented by pyrite, chalcopyrite, sphalerite, galena, argentite, covelite and electrum. Gold and silver minerals increase where sulfides are more abundant and the economic concentration of electrum and sulfide ores is more or less restricted to the black sulfide rich layers in the ore veins (Fig. 3A and B). High concentrations of molybdenum are strongly affected by Au-mineralization (Moon et al., 2010). Coexisting tellurium and tennantite are replaced by chalcopyrite. Goldfieldite, coexisting with hessite, is replaced by chalcopyrite along the grain margins. Gold occurs as fine <0.04 mm grains of electrum in sulfide minerals (83–87%Au, 8–15% Ag).

Ore veins in the Gasado deposits consist mainly of quartz and calcite with adularia, alunite, dickite, sericite, chlorite and sulfides. Fine grained sulfides including pyrite, sphalerite and chalcopyrite are disseminated in ore veins. Electrum is found mostly in the fine grained pyrites. Sericite is pervasive in the alteration zone, yielding a K–Ar age of 70.1–70.5 Ma (Koh et al., 2000).

2.4. Hydrothermal alteration

A hydrothermal alteration zone has developed around the ore veins of the Eunsan deposits and neighbouring areas, which is characterized by sericite, adularia and chlorite. Mineralized areas are dominated by argillic, prophylitic, sericitic and silicic alteration (Fig. 2). Advanced argillic alteration is lacking in the Eunsan mineralized zone. Potassic alteration is much more extensive relative to sericitization in the bonanza area of the Eunsan deposits (Aung, 2004). Alteration minerals at both Moisan and Eunsan deposits are dominated by sericite, which is closely associated with gold mineralization. Adularia is a characteristic mineral of low sulfidation ores and occurs as large sub- to euhedral or rhombic crystals by replacement of plagioclase (Kim, 2011). Propylitic alteration occurs in the outermost zone of both deposits (Fig. 2).

Four hydrothermal alteration zones in the Gasado deposit are recognized from the core of the vein to the periphery: an advanced argillic zone, argillic zone, phyllic zone and propylitic zone (Kim et al., 2002). Alunite-dickite clay mineral deposits are found at Ogmaesan, Sungsan and Ogchul mines (Fig. 1) located near the epithermal gold deposits as the result of local hydrothermal alteration (Choi et al., 2005). These deposits also provide information about both the temperature and origin of the epithermal gold deposits.

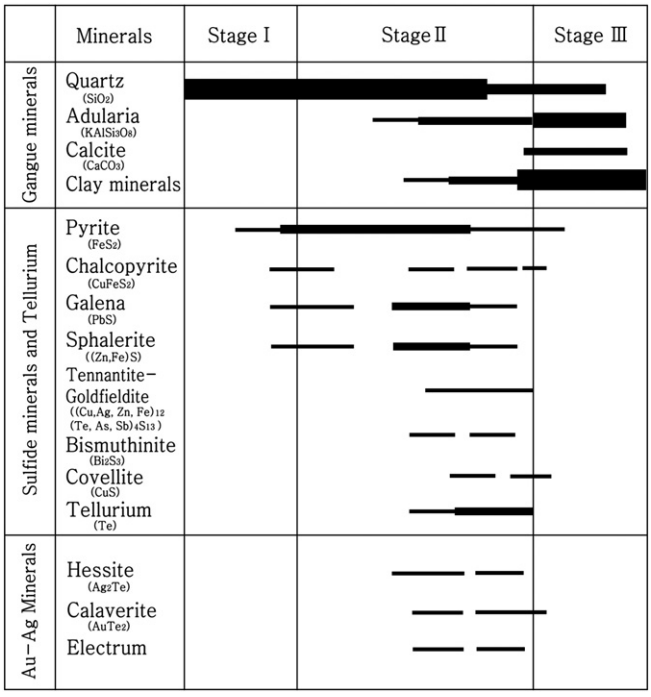

Fig. 4. Generalized paragenetic sequence for the Eunsan and Moisan gold-silver deposits (modified from Lee, 2011). Line width indicates abundances (thick: abundant, thin: less abundant).

3. Fluid inclusion study

3.1. Analytical method

A textural and microthermometric study has been made of fluid inclusions from the Eunsan and Moisan ores. All fluid inclusions studied are hosted by quartz vein minerals associated with sulfides. Many populations of fluid inclusions were too small (less than 5 μm in diameter) to permit detailed examination. The microthermometric determinations were made on doubly polished thin sections (80–100 μm thick) using a Linkam Th 600 heating/cooling stage at Pusan National University. The stage was calibrated at the triple points of CO_2 (−56.6 °C) and H_2O (0 °C) and at the critical point of H_2O (374.1 °C) using synthetic fluid inclusions (Shepherd et al., 1885). The freezing technique described by Haynes (1985) was employed over the expected temperature range. The accuracy and reproducibility of the temperature range of phase changes are approximately ±0.1 °C at $T \leq 50$ °C and ±0.5 °C at $T \leq 374.1$ °C. Salinities of aqueous inclusions, which were expressed as wt.% NaCl equiv., were calculated using the program SALTY (Bodnar et al., 1989). The volume fraction of liquid water in the fluid inclusions is defined according to the equation F = vol(liq)/vol(total) (Shepherd et al., 1885).

3.2. Fluid inclusion types and microthermometric data

Three major types of fluid inclusions can be recognized in the Sunshin ore deposits based on the number and volumetric proportion of phases present in the inclusions at room temperature (Fig. 5): (1) liquid-rich (type I) dominated by more than 50 vol.% of H_2O liquid at room temperature, (2) vapor-rich (type II) with less than 50 vol.% of H_2O liquid at room temperature and (3) CO_2-bearing multiphase (type III) inclusions that are characterized by a gas bubble within an aqueous liquid. Type I inclusions range in size up to 30 μm but are mostly less than 10 μm and exhibit ellipsoidal to irregular shapes (Fig. 5). The proportion of the vapor phase appears to be relatively constant in type II inclusions, irrespective of inclusion size (<40 μm). CO_2-bearing multiphase (type III) inclusions exhibit ellipsoidal to irregular shapes and are less than 30 μm in diameter (Fig. 5). Type III inclusions are probably of primary origin as demonstrated by their isolated distribution patterns.

Microthermometry of fluid inclusions trapped in ore vein quartz from the Sunshin gold deposits is summarized in Table 2. Homogenization temperatures vary from 136 to 231 °C for type I inclusions. Salinities, determined by freezing point depression (Bodnar, 1993), were 0.5 to 6.2 wt.% NaCl equiv. for inclusions trapped within quartz. Homogenization temperatures of type II inclusions vary from 146 to

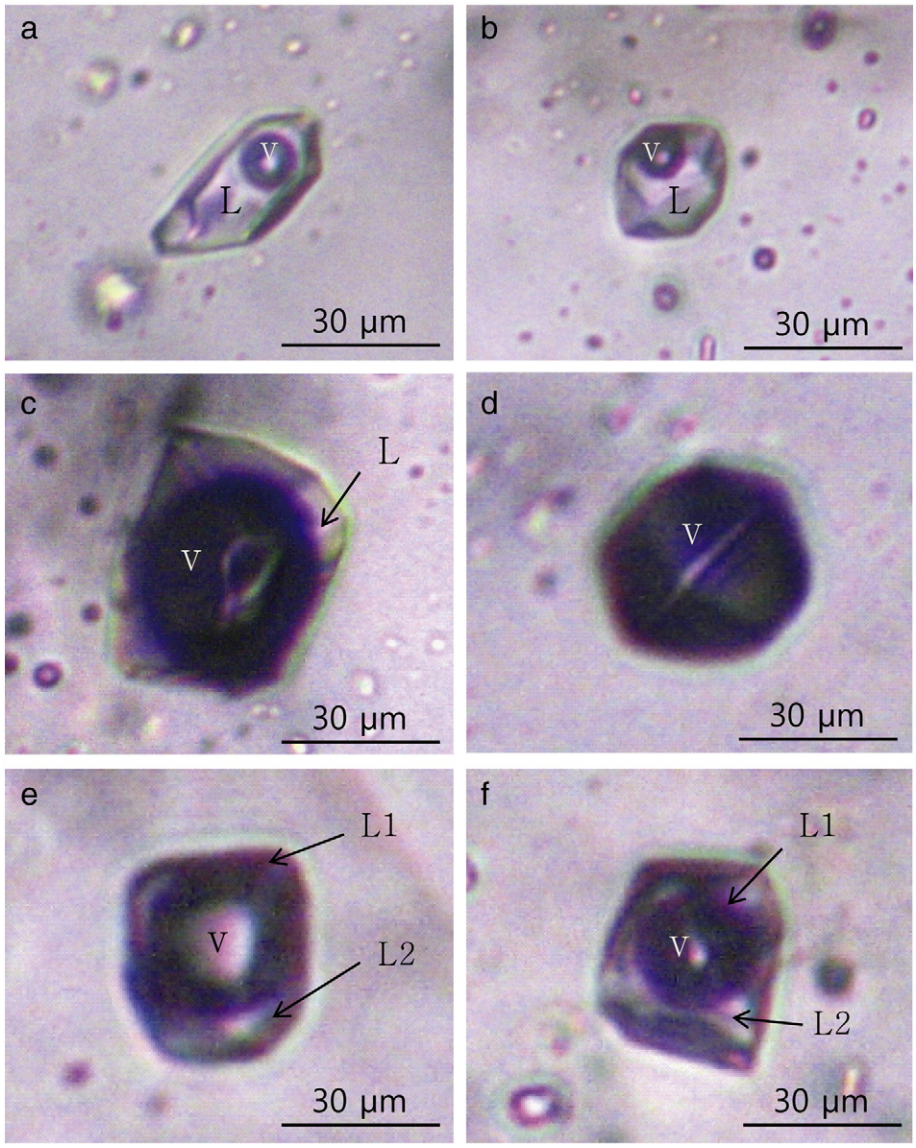

Fig. 5. Photomicrographs of different types of fluid inclusions in ore vein quartz from the Sunshin gold deposits. Type I liquid-rich inclusion (a, b), Type II vapor-rich inclusion (c, d), Type III CO_2-bearing inclusion (e, f). L: liquid, V: vapor.

310 °C, but our measurement of type II inclusions may be limited by the density of H_2O fluid being lower than the critical point (0.32 g/cm^3). Final ice melting occurred at temperatures above −0.6 to 3.7 °C for all measured type II inclusions, indicating a low salinity (1.0–4.7 wt.% NaCl equiv.). Type III inclusions yield relatively low homogenization temperatures ranging from 160 °C to 210 °C. Evidence from fluid inclusions suggests the epithermal environment of gold ore precipitation in the Sunshin deposits was shallow (pressure <150 bars, Table 2).

4. Isotope studies

4.1. Analytical methods

Seven stainless-steel tubes with metal valves were connected to a noble gas purification line. Samples of mineral separates, weighing 0.5-1 g each, and nickel rods were separately installed in each tube. The samples were heated overnight at 150 °C under an ultra-high vacuum to remove atmospheric noble gas contamination. Noble

Table 2
Summary of microthermometry of fluid inclusions trapped in vein quartz from the Sunshin gold deposits.

Location	Type	Te (°C)	Tm $_{ice}$ (°C)	Th$_{CO2}$ (°C)	Tm$_{vapor}$ (°C)	Th$_{total}$ (°C)	P(bars)*	Salinity (wt.% NaCl)
Eunsan	Type I	−49 to −33	−3.8 to −0.3		136–261	136–261	30–150	0.5–6.2
	Type II	−47 to −36	−3.0 to −0.6		238–310	238–310	100–150	1.0–4.5
	Type III			20–21	160–193	160–193		
Moisan	Type I	−39 to −34	−3.0 to −0.5		164–235	164–235	50–120	0.9–5.0
	Type II	−39 to −38	−2.8 to −1.6		146–289	146–289	40–150	2.7–4.7
	Type III			21–23	168–210	168–210		

Te: temperature of eutectic; Tm$_{ice}$: final ice melting temperature; Th$_{CO2}$: temperature of CO_2 homogenization; Tm$_{vapor}$: temperature of vapor disappearance, Th$_{total}$: temperature of total homogenization. *Calculated pressure from phase equilibria P–T relation diagram (Atkinson, 2002). Salinity is expressed in wt.% NaCl equivalent.

gases were extracted from the quartz and pyrite minerals in the ores using the in vacuo crushing method applied by Sumino et al. (2001). In the crushing experiments, ca. 0.5–1 g of samples were crushed in the stainless-steel tube by 2000 strokes of the nickel rod driven from outside the vacuum by a solenoid magnet. For two samples, 08SR01 and GS-02-01, gas was released by an additional 2000 strokes carried out after analysis of the first crushing step. During crushing of a sample, the metal valves for other samples were closed to avoid cross contamination among the samples.

Isotopic compositions of the released noble gases were measured with a sector-type mass spectrometer, a modified-VG5400 (MS-III) in the Geochemical Research Center, University of Tokyo, Japan. Sensitivities and discrimination factors for noble gas isotopes, except for $^3He/^4He$, were determined by measuring known amounts of atmosphere. The mass discrimination factor for $^3He/^4He$ was determined using HESJ (the He Standard of Japan), with $^3He/^4He = (28.88 \pm 0.14) \times 10^{-6}$ (Matsuda et al., 2002). Blank levels, measured using an empty tube with the same procedure applied to samples, were 2.4×10^{-11} (^4He), 1.7×10^{-12} (^{20}Ne), 1.7×10^{-9} (^{40}Ar), 3.6×10^{-13} (^{84}Kr), and 5.0×10^{-14} (^{132}Xe) in units of cm^3STP. The noble gas data obtained are summarized in Table 3. Experimental uncertainties in the noble gas concentrations were estimated to be about 10% based on the reproducibility of measurements of a standard air sample stored in a metal container attached to the purification line. Errors on isotopic ratios incorporate errors in blank correction and mass discrimination and are quoted at one standard deviation.

For oxygen and hydrogen isotopic analysis, oxygen from Au bearing vein quartz was liberated by reaction with BrF_5 in Ni bombs at higher temperatures (650–700 °C) over 24 hours (Clayton and O'Neil, 1972). The oxygen yield (95–100%) was converted to CO_2 by reaction with a hot carbon rod. Hydrogen from fluid inclusions in quartz and calcite minerals was liberated by reaction with hot zinc metal to produce H_2 for analysis (Coleman et al., 1982). Oxygen and hydrogen isotopic ratios were measured in a Finnigan Delta-E mass spectrometer at the Institute of Mineral Deposits, Chinese Academy of Geological Sciences, China. The analytical precisions were ±0.1‰ for $\delta^{18}O$ and ±2‰ for δD.

4.2. He isotopes

The concentrations of ^4He are $(0.6–147) \times 10^{-9}$ cm^3STP/g and the $^3He/^4He$ ratios for the studied areas, Sunshin, Tongyoung, and Kwangyang, range from $(0.15 \pm 0.03)R_A$ to $(9 \pm 2)R_A$. The ^4He concentrations in pyrite samples are generally higher than those in quartz samples, but the range of $^3He/^4He$ ratios is much narrower, $0.24–2.7R_A$, in pyrite samples compared with 0.15 to $9R_A$ in quartz samples. On the other hand, such a difference in Ar compositions between pyrite and quartz samples is not found. High $^3He/^4He$ ratios close to the MORB value ($8–10R_A$: Graham, 2002) are observed for the samples with relatively low concentrations of He. Cosmogenic ^3He can be considered negligible for the samples with high ratios because these were all collected from drill cores or underground mining sites.

4.3. Ar isotopes

^{40}Ar concentrations and isotopic data for gas from fluid inclusions from the Sunshin epithermal gold deposits are listed in Table 3. Concentrations of ^{40}Ar are $(62–1485) \times 10^{-9}$ cm^3STP/g and the $^{40}Ar/^{36}Ar$ ratios range from 297 to 419 for the Sunshin samples. The $^{40}Ar/^{36}Ar$ ratios are close to the atmospheric value of 296 with a small amount of excess ^{40}Ar. The $^{40}Ar/^{36}Ar$ ratios in pyrite ($^{40}Ar/^{36}Ar = 299–315$) are quite similar to those of quartz ($^{40}Ar/^{36}Ar = 297–332$), implying the minerals formed under similar conditions. The $^{40}Ar/^{36}Ar$ ratios from Tongyoung and Kwangyang gold deposits are 310.3 and 477–728, respectively, which are slightly higher than those of the Sunshin samples.

Table 3
Noble gas isotopic compositions of fluid inclusions in quartz from the Sunshin epithermal gold-silver ore deposits of the Haenam metallogenic province.

Sample no.	Weight g	Mineral[a]	Concentrations				$^4He/^{20}Ne$	Isotopic ratios		
			^3He	^4He	^{36}Ar	^{40}Ar		$^3He/^4He$	$^{38}Ar/^{36}Ar$	$^{40}Ar/^{36}Ar$
			$10^{-15}cm^3STP/g$	$10^{-9}cm^3STP/g$	$10^{-9}cm^3STP/g$			R/RA[c]		
Eunsan deposit										
Sn-2	0.5289	Qz	12 ± 2	2.69 ± 0.30	0.22 ± 0.02	64 ± 7	0.38	4.13 ± 0.75	0.1865 ± 0.0010	297.4 ± 0.6
Sn-3	0.7957	Py	499 ± 52	147 ± 15	0.58 ± 0.06	174 ± 18	181	2.42 ± 0.06	0.1871 ± 0.0013	299.2 ± 0.9
08SR03	1.0482	Py	112 ± 12	82.9 ± 8.3	0.58 ± 0.06	176 ± 18	212	0.96 ± 0.04	0.1873 ± 0.0008	305.6 ± 0.5
08SR01 CR1[b]	1.0317	Qz	4.1 ± 1.3	2.87 ± 0.29	0.66 ± 0.07	203 ± 20	3.97	1.02 ± 0.32	0.1878 ± 0.0008	306.3 ± 0.8
08SR01 CR2[b]	1.0317	Qz	5.9 ± 1.2	1.53 ± 0.15	0.19 ± 0.02	62 ± 6	5.72	2.75 ± 0.48	0.1870 ± 0.0010	328.7 ± 1.1
08SR04	0.7688	Qz	6.6 ± 1.7	1.39 ± 0.14	3.15 ± 0.32	980 ± 98	0.483	3.40 ± 0.81	0.1865 ± 0.0014	311.4 ± 2.7
08SR03	0.9464	Qz	3.6 ± 1.2	12.5 ± 1.3	0.96 ± 0.10	297 ± 30	12.3	0.21 ± 0.07	0.1882 ± 0.0008	309.8 ± 0.5
08SR04	1.0230	Py	103 ± 13	74.2 ± 7.4	0.92 ± 0.09	283 ± 28	111	1.00 ± 0.07	0.1881 ± 0.0007	308.5 ± 0.4
Moisan deposit										
09SR19	0.9135	Qz	9.2 ± 2	0.96 ± 0.10	1.93 ± 0.19	588 ± 59	0.393	6.9 ± 1.3	0.1886 ± 0.0009	304.6 ± 0.8
09SR01	0.5761	Py	25 ± 4	73 ± 7	0.53 ± 0.05	167 ± 17	131	0.24 ± 0.03	0.1862 ± 0.0010	315.1 ± 1.1
09SR07	0.8839	Qz	5.5 ± 1.2	25.7 ± 2.6	0.54 ± 0.05	178 ± 18	66.8	0.15 ± 0.03	0.1888 ± 0.0019	332.0 ± 2.7
Sn-1	0.5666	Qz	16 ± 2	3.05 ± 0.31	0.87 ± 0.09	274 ± 28	7.16	3.9 ± 0.3	0.1876 ± 0.0007	315.8 ± 0.8
Gasado deposit										
GS-02-01 CR1[b]	0.9490	Qz	8.8 ± 2.6	1.31 ± 0.13	0.44 ± 0.04	158 ± 16	3.35	4.8 ± 1.4	0.1893 ± 0.0012	357.1 ± 0.9
GS-02-01 CR2[b]	0.9490	Qz	7.9 ± 3.4	0.937 ± 0.095	0.20 ± 0.02	85 ± 9	5.04	6.0 ± 2.5	0.1886 ± 0.0016	419.2 ± 1.3
GS-03-2	0.9448	Qz	7.3 ± 1.9	0.59 ± 0.06	4.89 ± 0.49	1485 ± 156	0.09	8.9 ± 2.2	0.1882 ± 0.0036	303.5 ± 10
GS-03-1	0.9432	Qz	5.3 ± 1.4	0.61 ± 0.06	1.55 ± 0.16	502 ± 50	0.426	6.3 ± 1.5	0.1868 ± 0.0011	323.5 ± 0.8
GS-02-2	0.9269	Qz	5.0 ± 1.7	5.92 ± 0.59	1.28 ± 0.13	411 ± 41	5.92	0.61 ± 0.19	0.1854 ± 0.0012	320.7 ± 1.1
Tongyoung[d]										
Ty-1	0.5194		16 ± 2	10.4 ± 1.0	2.32 ± 0.23	720 ± 72	7.77	1.16 ± 0.12	0.1896 ± 0.0006	310.3 ± 0.5
Kwangyang[d]										
Ky-1	0.5343	Qz	25 ± 5	15.7 ± 1.6	1.18 ± 0.12	858 ± 87	9.8	1.24 ± 0.18	0.1883 ± 0.0011	728.4 ± 2.1
Ky-2	0.7045	Py	198 ± 21	52.7 ± 5.3	0.49 ± 0.05	233 ± 24	257	2.69 ± 0.08	0.1843 ± 0.0021	477.5 ± 2.9

[a] Qz: quartz, Py: pyrite.
[b] CR1: crush 1, CR2: crush 2.
[c] $R/R_A = (^3He/^4He)_{sample}/(^3He/^4He)_{Air}$, where $(^3He/^4He) = 1.4 \times 10^{-6}$.
[d] Epithermal type gold deposits measured for comparison (see text).

Table 4
Oxygen and hydrogen isotopic ratios of quartz and calcite minerals from the Sunshin epithermal Au–Ag deposits.

Sample no.	Mineral	$\delta^{18}O_{SMOW}$(‰)	$\delta^{18}D_{SMOW}$(‰)	$\delta^{18}O_{SMOW}$(‰)		
				(Water) at 250 °C	(Water) at 200 °C	(Water) at 150 °C
08SR01	Quartz	5.7	−94	−3.2	−6.0	
08SR03	Quartz	5.1	−85	−3.8	−6.6	
08SR04	Quartz	7.0	−100	−1.9	−4.7	
09SR01	Quartz	6.3	−91	−2.6	−5.4	
09SR07	Quartz	5.9	−87	−3.0	−5.8	
09SR08	Quartz	5.8	−97	−3.1	−5.9	
09SR19	Quartz	5.9	−82	−3.0	−5.8	
08SR01	Calcite	2.3	−94		−6.7	−9.8
09SR01	Calcite	2.0	−100		−7.0	−10.1
09SR07	Calcite	2.1	−97		−6.9	−10.0

1000 ln $\alpha_{quartz\text{-}water} = -3.31 + 3.34\ (10^6/T^2)$ at 250 °C (Clayton et al., 1972).
1000 ln $\alpha_{quartz\text{-}water} = -3.40 + 3.38\ (10^6/T^2)$ at 200 °C (Campbell and Larson, 1998).
1000 ln $\alpha_{calcite\text{-}water} = -3.39 + 2.78\ (10^6/T^2)$ at 150 °C and 200 °C (O'Neil and Taylor, 1969).

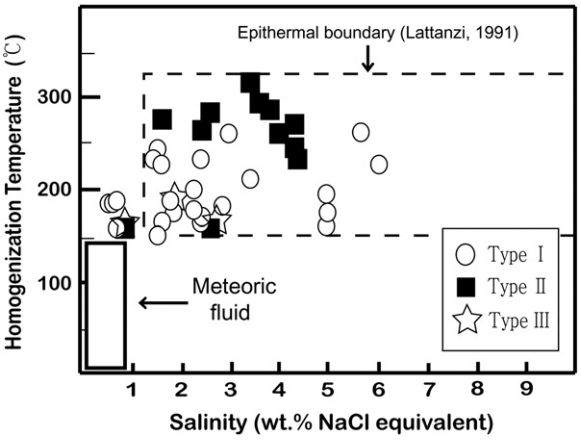

Fig. 7. Salinity vs. homogenization temperature diagram for fluid inclusions in quartz from the Sunshin gold mine. The hypothetical compositions of meteoric waters are plotted according to Naden et al. (2005) and Lattanzi (1991).

4.4. Oxygen and hydrogen isotopes

Oxygen and hydrogen isotope analyses were performed on seven quartzes and three calcites from the Moisan and Eunsan ore deposits. The $\delta^{18}O$ results for ore quartz have a relatively narrow range of values from 5.1 to 7.0‰. Their hydrogen isotopic ratios (δD) fall between −82 and −100‰ (Table 4). The $\delta^{18}O$ values for ore quartz from the Gasado deposits range from −8.0 to −10.1‰. The δD values of the extracted fluids range between −64 and −68‰ (Kim et al., 2002). As shown in Fig. 8, the isotopic range of the Gasado deposits is significantly different from that of the other Sunshin deposits, strongly suggesting a different hydrothermal source.

Using the isotopic fractionation between quartz and water (Clayton et al., 1972; Campbell and Larson, 1998) at 150, 200, and 250 °C, the oxygen isotope ratios of the mineralizing fluids were calculated from the oxygen isotope composition of quartz (Table 4). Calculated $\delta^{18}O$ of ore fluids during quartz precipitation range from −3.8 to −1.9‰ at 250 °C and −6.6 to −4.7‰ at 200 °C (Clayton et al., 1972; Campbell and Larson, 1998). Calcites from ore quartz veins, formed in a later paragenetic sequence, have lighter isotopic compositions than quartz, ranging from 2.0 to 2.3‰ in $\delta^{18}O$ and −94 to −100‰ in δD. $\delta^{18}O$ of carbonate fluids were calculated to be −7.0 to −6.7‰ at 200 °C and −10.1 to −9.8‰ at 150 °C (O'Neil and Taylor, 1969) (Table 4). These values, which are significantly lower than those of magmatic water (5 to 9.5‰ in $\delta^{18}O$, -40 to −80‰ in δD; Ohmoto, 1986; Sheppard, 1986; Hedenquist and Lowenstern, 1994), indicate the strong influence of local paleo-meteoric waters in ore forming fluids of the Sunshin epithermal gold deposits.

5. Discussion

Fluids involved in the formation of epithermal deposits can have three main sources: magmatic fluids, deeply circulated meteoric waters (crustal waters), and shallow meteoric waters (Albinson et al., 2000). Hosono and Nakano (2004) proposed that, based on Nd-Sr-Pb isotopes, ore fluids of the Hishikari LSEOD, Japan, were derived from a mixture of magmatic and deep crustal fluids. On the basis of $\delta^{18}O$ and δD values, Yilmaz et al. (2007) also reported that mineralizing solutions were a mixture of meteoric and magmatic waters in the low sulfidation type Au–Ag mineralization at Bergama, Izmir, Turkey. On the other hand, Matsuhisa et al. (1985) reported that ore fluids of

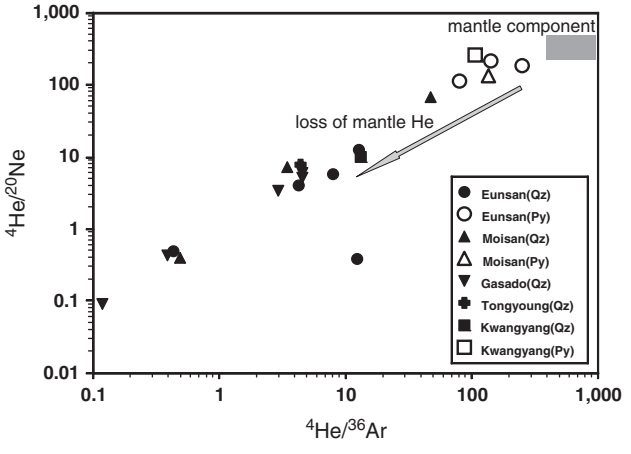

Fig. 6. $^4He/^{20}Ne$ vs. $^4He/^{36}Ar$ of inclusion-trapped fluids in ore quartz and pyrite samples. Large and small symbols represent noble gas data for pyrite and quartz samples, respectively. The noble gases would have originated from the mantle transported by magmatic fluids and then trapped within fluid inclusions. The plots clearly show that the quartz samples are heavily depleted in He compared with the pyrite samples. Accordingly, He in pyrite is a more reliable measure to use than He in quartz when discussing the origin of He during ore formation. Mantle noble gas component derived from Ozima and Podosek (2002).

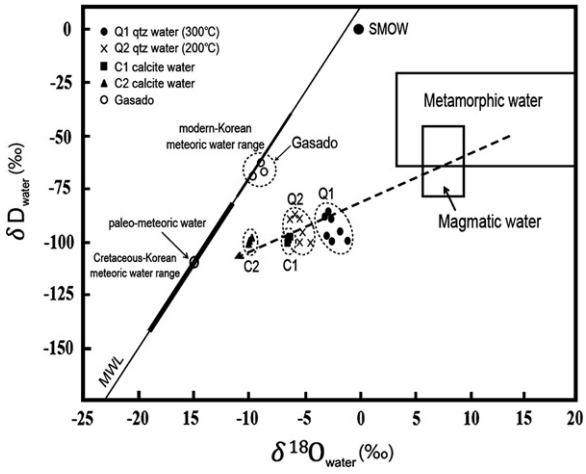

Fig. 8. Plot of δD vs. calculated $\delta^{18}O$ for waters from the Sunshin gold deposits. The dotted circle represents the calculated oxygen isotopic composition of water in equilibrium with quartz and calcite at the indicated temperatures on the top left. The arrow indicates a progressive influx of meteoric water into magmatic water. The metamorphic and magmatic water boxes are from Taylor (1979). MWL = Meteoric water line. SMOW = Standard Mean Ocean Water. Gasado data from Kim et al.(2002).

Au–Ag LSEOD are predominantly comprised of meteoric water with little indication of a magmatic component. Therefore, stable isotopic data do not yield an unequivocal explanation of the origin of ore fluids in LSEOD.

Unlike stable isotopes, He isotopic composition has proven to be an excellent discriminator of different fluid sources. Helium in ore forming fluids has only two possible sources: the mantle or radiogenic ^{4}He produced in the crust (Turner et al., 1993). The concentration of helium in the atmosphere is too low to exert a significant influence on He abundances and the isotopic composition of most crustal fluids (Stuart et al., 1994). Therefore, the He in the ore fluids that generated the Sunshin gold ores is predominantly non-atmospheric in origin. The ^{3}He/^{4}He ratios of crustal helium and upper mantle are $<0.05R_A$ (Mamyrin and Tolstikhin, 1984; Turner et al., 1993) and $\sim 8.5R_A$ (Graham, 2002), respectively. Hence a more powerful tool to further characterize the origin of fluids in hydrothermal ore deposits, especially in epithermal types, relies on the combined use of stable isotopes and helium isotopic ratios (e.g., Hedenquist and Aoki, 1991; Albinson et al., 2000; Moore et al., 2001; Camprubi et al., 2006).

5.1. Helium and argon isotopic ratios of the fluid inclusions

Fig. 6 depicts plots of ^{4}He/^{20}Ne vs. ^{4}He/^{36}Ar of inclusion-trapped fluids in ore quartz and pyrite samples from the studied area. The decreasing trend in both the ^{4}He/^{20}Ne and ^{4}He/^{36}Ar ratios from the mantle component represents a loss of He from the samples. The plots clearly show that the quartz samples are heavily depleted in He compared with the pyrite samples. ^{40}Ar/^{36}Ar ratios are plotted against ^{3}He/^{36}Ar in Fig. 9. Most of the ^{3}He/^{36}Ar ratios in the quartz samples are much lower than those in the pyrite samples. This also indicates a loss of mantle He from the fluid inclusions through their host quartz, because ^{3}He should have mostly originated from the mantle. The low ^{40}Ar/^{36}Ar ratios shown in Fig. 9 were probably due to dilution of mantle derived noble gases by atmospheric noble gases dissolved in meteoric water at shallow depths in the crust during ore formation as will be discussed in following sections. The better retentivity of He in pyrite compared to quartz samples, as shown in Figs. 6 and 9, indicates that ^{3}He/^{4}He ratios in pyrite are a more reliable measure to use when discussing the origin of He during ore formation, although there were a smaller number of pyrite samples than quartz samples measured.

Fig. 10 shows plots of ^{3}He/^{4}He vs. ^{40}Ar*/^{4}He in ore quartz and pyrite samples following the figure of Stuart et al. (1995). Excess ^{40}Ar concentration, ^{40}Ar*, compared with the atmospheric ^{40}Ar/^{36}Ar = 296 was calculated by the formula in the caption. The higher ^{40}Ar*/^{4}He ratios for quartz samples compared with pyrite ones might have resulted from greater loss of He from the quartz fluid inclusions through their host. ^{40}Ar*/^{4}He for pyrite samples can be explained by mixing of a MORB-like mantle gas with a crustal one. On the other hand, the noble gas composition of inclusions in quartz might have resulted from diffusive loss of He and then admixing of crustal ^{4}He and ^{40}Ar*. Diffusive He loss will cause the ^{3}He/^{4}He ratio of residual He in inclusions to decrease due to the faster diffusion of ^{3}He compared with ^{4}He in host minerals (e.g., Craig and Lupton, 1976; Trull et al., 1991). The reduction of ^{3}He/^{4}He ratios from MORB-like He ($10R_A$) following Rayleigh fractionation can be calculated (e.g., Ozima and Podosek, 2002). Loss of 90% ^{4}He causes a 30% ($6R_A$) reduction in ^{3}He/^{4}He ratio, 99% ^{4}He loss causes a ~50% ($4R_A$) reduction, and a 99.9% loss causes a 66% ($3R_A$) reduction. The scale of reduction in our samples seems to be ca. 1–10%. The reduction in ^{3}He/^{4}He ratio is indicated in Fig. 10.

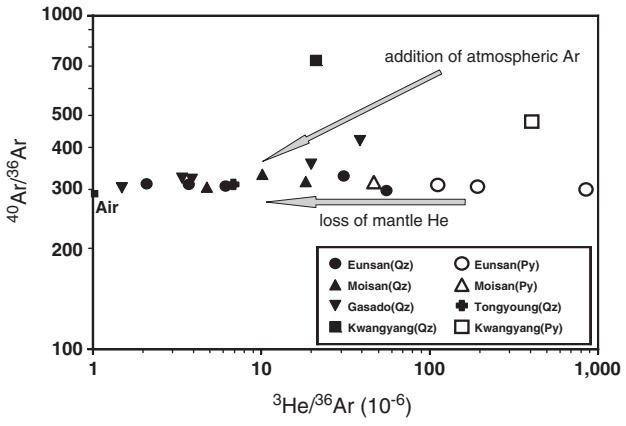

Fig. 9. ^{40}Ar/^{36}Ar vs. ^{3}He/^{36}Ar of inclusion-trapped fluids in ore quartz and pyrite samples. The lower ^{3}He/^{36}Ar in quartz than in pyrite would have resulted by diffusive He loss from quartz. The low ^{40}Ar/^{36}Ar ratios were probably due to dilution of mantle derived noble gases with atmospheric noble gases dissolved in meteoric water during ore formation at shallow crustal depths (see text). Figure modified after Stuart et al. (1995).

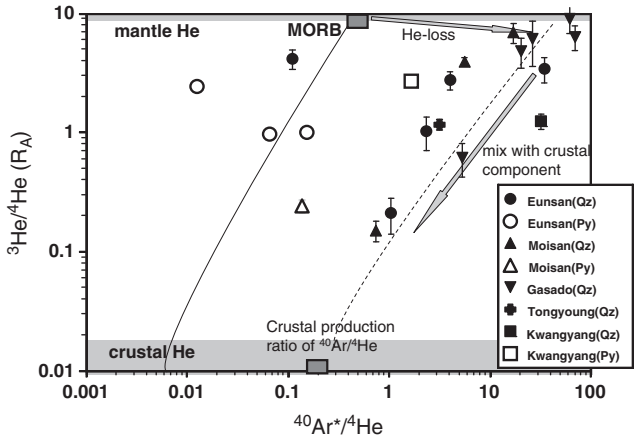

Fig. 10. ^{3}He/^{4}He vs. ^{40}Ar*/^{4}He of inclusion-trapped fluids in ore quartz and pyrite samples. Excess ^{40}Ar concentration, ^{40}Ar*, compared with the atmospheric ^{40}Ar/^{36}Ar = 296 was calculated by $^{40}\text{Ar}^* = (^{40}\text{Ar}/^{36}\text{Ar} - 296) \times {}^{36}\text{Ar}$. Helium and Ar in pyrite can be explained as a mixture between MORB-like mantle gas and crustal gas. On the other hand, the noble gas composition of fluid inclusions in quartz might have resulted from diffusive He loss and then admixing of crustal ^{4}He and ^{40}Ar. The results suggest that the He trapped in fluid inclusions was originally mantle-derived with ^{3}He/^{4}He $\sim 8.5R_A$ (Graham, 2002). Figure modified after Stuart et al. (1995).

Although ^{3}He/^{4}He ratios in the Eunsan and Moisan pyrites, (0.24–2.4)R_A, are not as high as the mantle value of $\sim 8.5R_A$, they are much higher than the crustal value of $<<0.1R_A$. This suggests that the He supplied to the ore forming region by fluids was originally mantle-derived. The mineralization age of the deposits is less than 90 Ma and an assumed maximum U concentration in the fluid inclusions is less than 4 ppm (Hu et al., 1998; Burnard et al., 1999). Maximum production of ^{4}He from U under these conditions becomes $44{,}000 \times 10^{-9}$ cm^{3}STP/g, which are two orders of magnitude larger than the observed large values for pyrites. Hence, addition of only a small fraction of such radiogenic ^{4}He can easily decrease the ^{3}He/^{4}He ratio of mantle-derived He. The quartz samples provide minimum estimates for the ^{3}He/^{4}He ratios because both processes, diffusion loss and addition of radiogenic ^{4}He, would have lowered the ratios. Hence, the quartz samples also show mantle-derived He for the ore forming fluids although experimental errors are large due to the low concentrations of He in these samples.

On the other hand, Yamamoto et al. (2004) pointed out that as pyrite is a suitable trap for noble gases (Stuart et al., 1994; Burnard et al., 1999; Hu et al., 2004), Rayleigh fractionation can be ruled out to explain the observed low ^{3}He/^{4}He ratios. If this is the case for the ore deposits in the Sunshin area, then radiogenic ^{4}He accumulated and released from crustal rocks surrounding the ore deposits, had already mixed with low ^{3}He/^{4}He ratio fluids prior to ore deposition and

evidence of this mixing is preserved in fluid inclusions. The observed $^{3}He/^{4}He$ ratios in pyrite and quartz from ore veins, 0.15-9R_A, are overlapped by those of mantle xenoliths (3.5 to 7.9R_A in $^{3}He/^{4}He$, Kim et al., 2005) from the Korean peninsula. Hence the He isotope evidence provides direct support to the theory linking magma from a mantle source and the LSEOD gold bearing fluids.

$^{40}Ar/^{36}Ar$ ratios for Sunshin gold deposits are relatively low with uniform values of 297–419 (av., 321), close to the atmospheric value of 296. Contributions to the measured $^{40}Ar/^{36}Ar$ from ^{40}Ar produced *in situ* from the mineral lattice and *in situ* via radiogenic growth in the fluid inclusions are thought unlikely due to the low diffusivity of Ar in quartz and pyrite and the absence of the parent isotope K in pyrite and quartz (York et al., 1982; Turner and Wang, 1992; Qiu, 1996; Smith et al., 2001). Compared with the Sunshin samples, fluid inclusions in quartz from Jurassic and Cretaceous granites in South Korea have much higher $^{40}Ar/^{36}Ar$ ratios of 1040 and 424, respectively (Kim et al., 2010). The Eunsan, Moisan and Gasado deposits were formed in the Cretaceous Period, as already noted above. The argon isotopic signature of fluid inclusions from the ore deposits strongly indicates the contribution of vast amounts of atmospheric argon to the epithermal ore forming fluids in this area.

5.2. Stable isotope compositions show origin of fluids

Our stable isotope data for the Eunsan and Moisan ore deposits demonstrates a dominance of meteoric waters ($\delta^{18}O_{H2O} = -3.8$ to $-1.9‰$, $\delta D = -82$ to $-100‰$) with oxygen isotopic compositions of both water and rock modified to varying degrees by their mutual interaction. In the $\delta^{18}O_{H2O}$–δD diagram, isotopic data for the ore quartz from these deposits plots on the mixing line between magmatic water and paleo-meteoric water (Fig. 8). The ore fluids in the Sunshin were derived from paleo-meteoric fossil fluids in the Cretaceous sedimentary beds.

Oxygen and hydrogen stable isotopic data for the auriferous ore fluids ($\delta^{18}O = -10.1$ to $-8.0‰$, $\delta D = -68$ to $-64‰$, Kim et al., 2002) in the Gasado deposit plot directly on the meteoric water line (Fig. 8). But the Gasado deposits appear quite distinct from present day local meteoric water ($\delta^{18}O = -6.5‰$, $\delta D = -45.6‰$, Kim and Nakai, 1988). This strongly indicates that the composition of ore forming fluids approaches those of local unexchanged meteoric waters. It is interesting to note that the purely meteoric water dominant Gasado ore fluids are combined with the most MORB-like helium isotopic signatures. These unusual isotopic characteristics possibly indicate the presence of a concealed felsic intrusion close to the ore forming hydrothermal system, which is characterized by fluids dominated by meteoric water.

5.3. Homogenization temperatures deduced from microthermometry

Our microthermometric measurements for fluid inclusions in the Sunshin ore vein quartz indicate relatively low homogenization temperatures (136–310 °C), with low salinities (0.5–6.2 wt.% NaCl equiv.) of ore fluids at shallow depth. No positive correlation between homogenization temperature and salinity can be recognized for the inclusions, a common trend found in many intrusion-centered mineralizing systems around the world (Meinert et al., 1997; Xu and Lin, 2000) (Fig. 7). The low pressure of formation coupled with the low salinity and low temperature indicated by fluid inclusions results from epithermal fluids mixing with local paleo-meteoric water. Such water is thought to play an important role in the Au–Ag ore precipitation of ore minerals in the Sunshin hydrothermal system. Mixing of meteoric water with hydrothermal ore fluids leads to more rapid cooling and dilution of the hot acidic ore fluids. With decreasing temperature silica-rich fluids deposit Au bearing bisulfide complexes. A combination of decreasing temperature and pressure, as well as dilution of hydrothermal fluids, culminates in boiling and increasing pH, which is the main stage of gold mineralization in the Sunshin deposits.

Choi et al. (2005) also pointed out that the ore forming fluids, mostly derived from meteoric waters, evolved by boiling and mixing events at relatively low temperature (<300 °C) and very low salinity (<4.0 wt.% NaCl equiv.). Gold mineralization is closely associated with sulfide formation at temperatures between ca. 270 and 210 °C.

5.4. Origin of ore fluids and formation condition of LSEODs

In general, adularia-sericite epithermal Au–Ag ore deposits are typically formed within back-arc basins or rifts (Corbett, 2002). As shown in Fig. 2, the presence of a deep seated felsic intrusion can be proposed as a source of the hydrothermal system driving Au–Ag precipitation in the Sunshin LSEODs. Helium isotopic ratios measured for fluid inclusions show that Au–Ag bearing fluids, which formed most LSEODs in South Korea, were derived from mantle-related magmas.

Stable isotope studies show that as fluids ascend to shallow depth they were cooled with large volumes of meteoric water. This is consistent with the low $^{40}Ar/^{36}Ar$ ratios, which are close to atmospheric values. Argon derived from magma with high $^{40}Ar/^{36}Ar$ ratios would have been diluted with large amounts of atmospheric Ar dissolved in the meteoric waters. In contrast to Ar, atmospheric He could not affect the isotopic ratio of mantle-derived He because of both the relatively high concentrations of magmatic He in the Au–Ag bearing fluids and the low concentration of atmospheric He dissolved in meteoric water. The microthermometric measurements for fluid inclusions indicate relatively low temperatures (≤300 °C) for the formation of LSEODs.

6. Conclusion

Noble gas isotopes (He and Ar), stable isotopes (O, H) and microthermometric measurements have been used to discriminate the sources of ore forming fluid and to evaluate the genesis of the Sunshin Au–Ag ore deposits, South Korea. The Au–Ag bearing quartz veins of the Sunshin deposits are hosted in rhyolitic and tuffaceous rocks of Cretaceous age, which have undergone phyllic-adularia-carbonate alteration near the gold veins showing characteristic low sulfidation epithermal type mineral assemblages such as quartz, sericite, illite, adularia, pyrite, and calcite.

Homogenization temperatures of fluid inclusions from ore-bearing quartz range from 146 to 310 °C with low salinity (1.0–4.5 wt.% NaCl equiv.).

The stable isotope ($\delta^{18}O$, δD) data indicate that the ore forming fluids in the Sunshin epithermal system were strongly diluted by local paleo-meteoric waters in the Cretaceous non-marine Haenam-Jindo volcanic-sedimentary basin.

The He in the ore fluids, with large variations in $^{3}He/^{4}He$ ratios ($^{3}He/^{4}He = 0.15–9R_A$), was originally derived from a mantle source. Large amounts of radiogenic ^{4}He produced *in situ* in the crust were added to this fluid prior to ore deposition. This mantle helium signature provides direct evidence of the link between mantle magma and low sulfidation ore fluids in epithermal gold deposits.

Acknowledgments

We thank Dr. G. R. Sung, and Miss S. J. Paek for support during field studies at the Sunshin mine. The comments of Dr F. Stuart, and a constructive anonymous reviewer helped to improve our manuscript. The study was supported by the National Research Foundation of Korea (2009-0470-2-2) and partly by KOPRI project (PE12060) and by the Ministry of Knowledge Economy (KETEP grant 2011T100200317) to K. Yang.

References

Albinson, T., Norman, D.I., Cole, D., Chomiak, B.A., 2000. Controls on formation of low sulfidation epithermal deposits in Mexico: constraints from fluid inclusion and stable isotope data. In: Albinson, T., Nelson, C.E. (Eds.), New Mines and Discoveries in Mexico and Central America: Society of Economic Geologists Special Publication Series, v. 8, pp. 1–32.

Atkinson, A.B., 2002. A model for the PTX properties of H2O-NaCl. Unpublished M.S.Thesis, Virginia Tech, Blacksburg VA 133 pp.

Aung, M., 2004. Mineralogical and geochemical studies on the genesis of low-sulfidation epithermal Au – Ag deposit of Eunsan, Henam area, Korea. Ph. D. Dissertation, Seoul National University.

Bodnar, R.J., 1993. Revised equation and table for determining the freezing point depression of H_2O-NaCl solutions. Geochimica et Cosmochimica Acta 57, 683–684.

Bodnar, R.J., Sterner, S.M., Hall, D.L., 1989. Salty: A Fortran program to calculate compositions of fluid inclusions in the system NaCl-KCl-H_2O. Computers and Geosciences 15, 19–41.

Burnard, P.G., Polya, D.A., 2004. Importance of mantle derived fluids during granite associated hydrothermal circulation: He and Ar isotopes of ore minerals from Panasqueira. Geochimica et Cosmochimica Acta 68, 1607–1615.

Burnard, P.G., Hu, R.Z., Turner, G., Bi, X.W., 1999. Mantle, crustal and atmospheric noble gases in Ailaoshan gold deposit, Yunnam Province, China. Geochimica et Cosmochimica Acta 63, 1595–1604.

Campbell, A.R., Larson, P.B., 1998. Introduction to Stable Isotope Applications in Hydrothermal Systems. In: Richards, J.P., Larson, P.B. (Eds.), Techniques in Hydrothermal Ore Deposits Geology: Reviews in Economic Geology, 10, pp. 173–193.

Camprubi, A., Chomiak, B.A., Villanueva-Estrada, R.E., Canals, A., Norman, D.I., Cardellach, E., Stute, M., 2006. Fluid sources for the La Guitarra epithermal deposit (Temascaltepec district, Mexico): volatile and helium isotope analyses in fluid inclusions. Chemical Geology 231, 252–284.

Choi, S.G., Ryu, I.C., Pak, S.J., Wee, S.M., Kim, C.S., Park, M.E., 2005. Cretaceous epithermal gold-silver mineralization and geodynamic environment, Korea. Ore Geology Reviews 26, 115–135.

Chough, S.K., Kim, S.B., Chun, S.S., 1996. Sandstone/chert and laminated chert/black shale couplets, Cretaceous Uhangri Formation (Southwest Korea): depositional events in alkaline lake environments. Sedimentary Geology 104, 227–242.

Chun, S.S., Chough, S.K., 1995. The Cretaceous Uhangri Formation, SW Korea, Lacustrine margin facies. Sedimentology 42, 293–322.

Clayton, R.N., O'Neil, J.R., 1972. The use of bromine pentafluoride in the extraction of oxygen from oxides and silicates for isotopic analysis. Geochimica et Cosmochimica Acta 27, 43–52.

Clayton, R.N., O'Neil, J.R., Mayeda, T.K., 1972. Oxygen isotope exchange between quartz and water. Journal of Geophysical Research 77, 3057–3067.

Coleman, M.L., Sheppard, T.J., Durhan, J.J., Rouse, J.E., Moore, G.R., 1982. Reduction of water with zinc for hydrogen isotope analysis. Analytical Chemistry 54, 993–995.

Cooke, D.R., Simmons, S.F., 2000. Characteristics and genesis of epithermal gold deposits. Reviews in Economic Geology 13, 221–244.

Corbett, G., 2002. Epithermal gold for explorationists. Australian Institute of Geoscientists Journal-Applied Geoscientific Practice and Research in Australia 1–26.

Craig, H., Lupton, J.E., 1976. Primordial neon, helium, and hydrogen in oceanic basalts. Earth and Planetary Science Letters 31, 369–385.

Deyell, C.L., Rye, R.O., Landis, G.P., Dissig, T., 2005. Alunite and role of magmatic fluids in the Tambo-high sulfidation deposit, El Indio-Pascua belt, Chile. Chemical Geology 215, 185–218.

Giggenbach, W., 1997. The origin and evolution of fluids in magmatic-hydrothermal systems, In: Barnes, H.L. (Ed.), Geochemistry of hydrothermal ore deposits, 3rd edition. John Wiley & Sons, Inc., pp. 737–796.

Graham, D.W., 2002. Noble gas isotope geochemistry of mid-ocean ridge and ocean island basalts: characterization of mantle source reservoirs. In: Porcelli, D., Ballentine, C.J., Wieleer, R. (Eds.), Noble gases in geochemistry and cosmochemistry: Reviews in Mineralogy and Geochemistry, Vol. 47, pp. 247–317.

Haynes, F.M., 1985. Determination of fluid inclusion composition by sequential freezing. Economic Geology 80, 1436–1439.

Heald, P., Foley, N.K., Hayba, D.O., 1987. Comparative anatomy of volcanic-hosted epithermal deposits: acid-sulfate and adularia-sericite types. Economic Geology 82, 1–26.

Hedenquist, J.W., Aoki, M., 1991. Meteoric interaction with magmatic discharges in Japan and the significance of mineralization. Geology 19, 1041–1044.

Hedenquist, J.W., Lowenstern, J.B., 1994. The role of magmas in the formation of hydrothermal ore deposits. Nature 370, 519–527.

Hedenquist, J.W., Arribas Jr., A., Gonzalez-Urien, E., 2000. Exploration for epithermal gold deposits. Reviews in Economic Geology 13, 245–277.

Hosono, T., Nakano, T., 2004. Pb–Sr isotopic evidence for contribution of deep crustal fluid to the Hishikari epithermal gold deposit, southwestern Japan. Earth and Planetary Science Letters 222, 61–69.

Hu, R.Z., Burnard, P.G., Turner, G., Bi, X.W., 1998. Helium and argon systematics in fluid inclusions of Machangqing copper deposit in west Yunnan province, China. Chemical Geology 146, 55–63.

Hu, R.Z., Burnard, P.G., Bi, X.W., Zhou, M.F., Peng, J.T., Su, W.C., Wu, K.X., 2004. Helium and argon isotope geochemistry of alkaline intrusion-associated gold and copper deposits along the Red River–Jingshajiang fault belt, SW China. Chemical Geology 203, 305–317.

John, D.A., 2001. Miocene and early Pliocene epithermal gold-silver deposits in the northern Great Basin, western United States: characteristic, distribution, and relationship to magmatism. Economic Geology 96, 1827–1853.

Kim, C.S., 2011. Genesis of the Cretaceous low sulfidation epithermal Au – Ag deposit in the Haenam District, Republic of Korea: Implication for Se type (Eunsan) and Te type (Moisan). Ph. D. Dissertation, Korea University. 177pp.

Kim, I.J., Nagao, K., 1992. K – Ar ages of the hydrothermal clay deposits and the surrounding igneous rocks in southwest Korea. Journal of Petrological Society of Korea 1, 58–70.

Kim, K.H., Nakai, N., 1988. Isotopic compositions of precipitations and groundwaters in South Korea. Journal of Geological Society of Korea 24 (1), 37–46 (in Korean with English Abstract).

Kim, M.Y., Shin, H.J., 1989. Chemical composition of sphalerite relating to mineralization at the Tongyeong mine, Korea. Journal of the Korean Institute of Mining Geology 22 (2), 103–115.

Kim, C.S., Choi, S.G., Choi, S.H., Lee, I.W., 2002. Hydrothermal alteration and its genetic implication in the Gasado volcanic hosted epithermal gold-silver deposit: use in exploration. Journal of Mineralogical Society of Korea 15, 205–220 (in Korean with English Abstract).

Kim, K.H., Nagao, K., Tanaka, T., Sumino, H., Nakamura, T., Okuno, M., Lock, J.B., Youn, J.S., Song, J., 2005. He-Ar and Nd-Sr isotopic compositions of ultramafic xenoliths and host alkali basalts from the Korean peninsula. Geochemical Journal 39 (4), 341–356.

Kim, K.H., Nagao, K., Sumino, H., Lee, S.E., Lee, J.I., Choo, M.K., 2010. He – Ar Isotopic Signatures of the Mesozoic Granitoids in South Korea. EGU 2010–113 EGU General Assembly 2010: Geophysical Research Abstracts, vol. 12.

Koh, S.M., Takagi, T., Kim, M.Y., Naito, K., Hong, S.S., Sudo, S., 2000. Geological and geochemical characteristics of the hydrothermal clay alteration in South Korea. Resource Geology 50, 229–242.

Lattanzi, P., 1991. Applications of fluid inclusions in the study and exploration of mineral deposits. European Journal of Mineralogy 3, 689–700.

Lee, S., 2011. Gold mineralization and the related epithermal system of the Sunshin mine, Haenam. MS thesis, Pusan National University. 102pp. (Korean with English abstract).

Lee, S.Y., Yang, K.H., Jeon, B.G., Bak, G., Koh, S.M., Seo, J.R., 2009. Glass inclusion in quartz phenocrysts of tuff from Sunshin Au mining area, Haenam, Jeonnam. Journal of Petrological Society of Korea 18 (4), 337–348.

Mamyrin, B.A., Tolstikhin, I., 1984. Helium isotopes in Nature. Elsevier, Amsterdam. 267 pp.

Matsuda, J., Matsumoto, T., Sumino, H., Nagao, K., Yamamoto, J., Miura, Y.N., Kaneoka, I., Takahata, N., Sano, Y., 2002. The $^3He/^4He$ ratio of the new internal He standard of Japan (HESJ). Geochemical Journal 36, 191–195.

Matsuhisa, Y., Morishita, Y., Sato, T., 1985. Oxygen and carbon isotope variations in gold bearing hydrothermal veins in the Kushikino mining area, southern Kyushu, Japan. Economic Geology 80, 283–293.

Meinert, L.D., Hefton, K.K., Mayes, D., Tasiran, I., 1997. Geology, zonation, and fluid evolution of the Big Gossan Cu–Au skarn deposit, Ertsberg district, Irian Jaya. Economic Geology 92, 509–533.

Moon, H.S., Jeong, S.W., Song, Y.G., Park, Y.S., 1991. Wall rock alteration of the Haenam pyrophyllite deposit related to felsic volcanism, southern Korea. Journal of the Korean Institute of Mining Geology 24, 83–96 (in Korean with English Abstract).

Moon, D.H., Koh, S.M., Lee, G.J., 2010. Geochemistry of the Moisan epithermal gold-silver deposit in Haenam area. Economic and Environmental Geology 43 (5), 491–503.

Moore, J.N., Norman, D.I., Kennedy, B.M., 2001. Fluid inclusion gas compositions from an active magmatic–hydrothermal system: a case study of the Geysers geothermal fluids, USA. Chemical Geology 173, 3–30.

Morishita, Y., Nakano, T., 2008. Role of basement in epithermal deposits: the Kushikino and Hishikari gold deposits, southwestern Japan. Ore Geology Reviews 34, 597–609.

Naden, J., Killias, S.P., Darbyshire, D.P.F., 2005. Active geothermal system with entrained seawater as modern analogs for transitional volcanic-hosted massive sulphides and continental magmatic-hydrothermal mineralisation: the example of Milos island, Greece. Geology 33, 541–544.

Ohmoto, H., 1986. Stable isotope geochemistry of ore deposits. Reviews in Mineralogy 16, 491–559.

O'Neil, J.R., Taylor, H.P., 1969. Oxygen isotope equilibrium between muscovite and water. Journal of Geophysical Research 74, 6012–6022.

Ozima, M., Podosek, F.A., 2002. Noble gas geochemistry, 2nd edition. Cambridge University Press. 286 pp.

Park, M.E., Sung, K.Y., James, L.P., 2001. Au – Ag-Te mineralization by boiling and dilution of meteoric groundwater in the Tongyeong epithermal gold system, Korea: implications from reaction path modeling. Economic and Environment Geology 34 (6), 507–522.

Qiu, H.N., 1996. $^{40}Ar/^{36}Ar$ dating of the quartz samples from two mineral deposits in western Yunnan (SW China) by crushing in vacuum. Chemical Geology 127, 211–222.

Rainbow, A., Clark, A.H., Kyser, T.K., Francois, G., Gabory, F., Hodgon, C.J., 2005. The Pierina epithermal Au – Ag deposit, Ancash, Peru: paragenetic relationships, alunite textures, and stable-isotope geochemistry. Chemical Geology 215, 235–252.

Shelton, K.L., So, C.S., Hacusster, G.T., Chi, S.J., Lee, K.Y., 1990. Geochemical studies of the Tongyeong gold-silver deposits, Republic of Korea: evidence of meteoric water dominance in a Te-bearing epithermal system. Economic Geology 85, 1114–1132.

Shepherd, T.J., Rankin, A.H., Alderton, P.H.M., 1885. A practical guide to fluid inclusion studies. Blackie & Son Ltd., Glasgow & London. 240 pp.

Sheppard, S.M.F., 1986. Characterization and isotope variation in natural waters. Stable Isotopes in High Temperature Geological Processes: In: Valley, J.W., Taylor, H.P., O'Neil, J.R. (Eds.), Reviews in Mineralogy, 16, pp. 165–184.

Shikazono, N., 2003. Geochemical and tectonicmevolution of arc-backarc hydrothermal systems. Developments in Geochemistery, 8. Elsevier. 463 pp.
Sillitoe, R.H., 1987. Gold deposits in western Pacific island arcs: the magmatic connection. In: Keays, R.R., Ramsay, W.R.H., Droves, D.I. (Eds.), The Geology of Gold Deposits: their perspective in 1988: Economic Geology Monograph, v. 6, pp. 274–291.
Smirnov, V.I., Ginzburg, A.I., Grigoriev, V.M., Yakovlev, G.F., 1983. Studies of mineral deposits. Mir Publishers, Moscow. 228 pp.
Smith, P.E., Evensen, N.M., York, D., Szatmari, P., Oliveira, D.C., 2001. Single-crystal (super 40) Ar- (super 39) Ar dating of pyrite: no fool's clock. Geology 29, 403–406.
Stuart, F.M., Turner, G., 1992. Abundance and isotopic composition of the noble gases in fluid inclusions. Chemical Geology 101, 97–111.
Stuart, F.M., Turner, G., Duckworth, R.C., Fallick, A.E., 1994. Helium isotopes as tracers of trapped hydrothermal fluids in ocean-floor sulfides. Geology 22, 823–826.
Stuart, F.M., Burnard, P.G., Taylor, R.P., Turner, G., 1995. Resolving mantle and crustal contributions to ancient hydrothermal fluids: He – Ar isotopes in fluid inclusions from Dae Hwa W-Mo mineralisation, South Korea. Geochimica et Cosmochimica Acta 59, 4663–4673.
Sumino, H., Nagao, K., Notsu, K., 2001. Highly sensitive and precise measurement of helium isotopes using a mass spectrometer with double collector system. Journal of the Mass Spectrometry Society of Japan 49, 61–68.
Taylor, H.P., 1979. Oxygen and hydrogen isotope relationships in hydrothermal mineral deposits. In: Barnes, H.L. (Ed.), Geochemistry of Hydrothermal ore deposits. John Wiley, New York, pp. 236–277.
Trull, T.W., Kurz, M.D., Jenkins, W.J., 1991. Diffusion of cosmogenic ^{3}He in olivine and quartz: implications for surface exposure dating. Earth and Planetary Science Letters 103, 241–256.
Turner, G., Wang, S.S., 1992. Excess argon, crustal fluid and apparent isochrons from crushing K-feldspar. Earth and Planetary Science Letters 110, 193–211.
Turner, G., Burnard, P.B., Ford, J.L., Gilmout, J.D., Lyon, I.C., Stuart, F.M., 1993. Tracing fluid sources and interaction. Philosophical Transactions of the Royal Society of London, Series A 344, 127–140.
White, N.C., Hedenquist, J.W., 1990. Epithermal environments and styles of mineralization: variation and their causes, and guidelines for exploration. Journal of Geochemical Exploration 36, 445–474.
Xu, G., Lin, X., 2000. Geology and geochemistry of the Changlongshan skarn iron deposit, Anhui Province, China. Ore Geology Reviews 16, 91–106.
Yamamoto, J., Kaneoka, I., Nakai, S., Kagi, H., Prikhod'ko, V.S., Arai, S., 2004. Evidence for subduction-related components in the subcontinental mantle from low ^{3}He/^{4}He and ^{40}Ar/^{36}Ar ratio in mantle xenoliths from Far Eastern Russia. Chemical Geology 207, 237–259.
Yilmaz, H., Oyman, T., Arehart, G.B., Colakoglu, A.R., Billor, Z., 2007. Low-sulfidation type Au – Ag mineralization at Bergama, Izmir, Turkey. Ore Geology Reviews 32, 81–124.
York, D., Masliwec, A., Kuybida, P., Hanes, J.E., Hall, C.M., Kenyon, W.J., Spooner, E.T.C., Scott, S.D., 1982. ^{40}Ar/^{36}Ar dating of pyrite. Nature 300, 52–53.
Zhang, Z., Mao, J., Wang, Y., Pirajno, F., Liu, J., Zhao, Z., 2010. Geochemistry and geochronology of the volcanic rocks associated with the Dong'an adularia-sericite epithermal gold deposit, Lesser Hinggan Range, Heilongjiang province, NE China: constraints on the metallogenesis. Ore Geology Reviews 37, 158–174.